



Influence of plate length and plate cooling rate on solidification and microstructure of A356 alloy produced by oblique plate

N. K. KUND

Department of Mechanical Engineering, Indian Institute of Science, Bangalore 560012, India

Received 17 January 2014; accepted 19 June 2014

Abstract: A356 alloy melt solidifies partially when it flows down on an oblique plate cooled from bottom by counter flowing water. Columnar dendrites are continuously formed on the plate wall. Because of the forced convection, these dendrites are sheared off into equiaxed/fragmented grains and then washed away continuously by producing semisolid slurry at plate exit. Plate cooling rate provides required extent/amount of solidification whereas plate length enables necessary shear for producing semisolid slurry of desired quality. Slurry obtained is solidified in metal mould to produce semisolid-cast billets of desired microstructure. Furthermore, semisolid-cast billets are also heat-treated to improve surface quality. Microstructures of both semisolid-cast and heat-treated billets are compared. The effects of plate length and plate cooling rate on solidification and microstructure of billets produced by using oblique plate are illustrated. Three different plate lengths (200 mm, 250 mm, 300 mm) associated with three different heat transfer coefficients (1000, 2000 and 2500 W/(m²·K)) are involved. Plate length of 250 mm with heat transfer coefficient of 2000 W/(m²·K) gives fine and globular microstructures and is the optimum as there is absolutely no possibility of sticking of slurry to plate wall.

Key words: aluminum alloy; oblique plate; slurry; microstructure; plate length; plate cooling rate

1 Introduction

Semisolid metal processing (SSM) is an unmatched technology where metal is cast at semisolid state compared with usual casting where metal is straightway cast from liquid state. SPENCER et al [1] investigated the rheological behavior of Sn–15%Pb binary alloy in the crystallization range by using a Couette type viscometer. The studies on the deformation behavior of Sn–15%Pb semisolid alloy have also been presented [2]. The influences of vibration during solidification have been investigated as well [3]. FLEMINGS [4] studied the behavior of metal alloys in the semisolid state. KIRKWOOD [5] discussed about the semisolid metal processing. FAN [6] illustrated clearly about semisolid metal forming technology. Investigations on the influence of isothermal mechanical stirring on an Al–Si alloy in the semisolid condition have been presented [7]. The effect of stirring on solidification pattern and alloy distribution during semi-solid metal casting has also been reported [8]. An outline about the implication of rheology in semisolid metal processing has been reported as well [9]. KUMAR [10] studied experimentally the

rheocasting of A356 aluminum alloy using linear electromagnetic stirring. BARMAN [11] numerically studied transport phenomena during solidification in presence of electromagnetic stirring. The influence of mechanical vibration of metal mould on the production of thixotropic feedstock of A356 aluminum alloy has also been reported [12].

Besides, numerical investigations on the hydrodynamic and thermo-solutal behavior of flowing down partially solidifying A356 alloy melt have been presented [13]. The scaling analysis of the problem has also been reported [14]. These investigations are theoretical in nature and do not in any way light up on the final microstructure. The particulars of solidification and microstructure can be found only through the rigorous experiments.

From the aforesaid studies, to the best of authors' knowledge, it is evident that there is not a single complete experimental study involving the effects of plate length and plate cooling rate on quality of semisolid slurry, solidification and microstructure of cast billets produced by an oblique plate. With this standpoint, the present work describes experimental studies with an oblique plate (on A356 aluminum alloy melt) concerning

the influences of plate length and plate cooling rate on quality of semisolid slurry, solidification and microstructure. Additionally, the studies also relate to isothermal holding of semisolid cast billets to produce heat-treated billets with superior surface quality. Lastly, to itemize and quantify the heterogeneity in microstructural morphology (for getting the desired microstructures), both semisolid-cast and heat-treated billets are examined and compared by using optical microscopy and image analysis technique.

2 Experimental

2.1 Materials

In the present investigation, A356 aluminum alloy ingots of liquidus temperature 618 °C, solidus temperature 555 °C and composition [10] as given in Table 1 are used for conducting experiments.

Table 1 Composition of A356 alloy (mass fraction, %)

Si	Mg	Fe	Mn	Cu	Ti	Al
7.32	0.31	0.086	≤0.010	≤0.010	0.157	Bal.

2.2 Melt preparation and treatment

Prior to each experiment, around 20 kg of A356 aluminum alloy ingot is melted at around 720 °C in a mica glazed silicon carbide crucible kept in a tilting electric resistance furnace. Once the metal reaches molten stage, the molten alloy is held for about 45 min at 720 °C, to allow for achieving temperature uniformity and full dissolution of alloying elements. This is then followed by the addition of predetermined quantities of grain modifiers (i.e., aluminum–strontium (Al–Sr) master alloy amounting to 0.25% of the total melt mass of the alloy) and refiners (i.e., titanium–boron (Ti–B) tablet amounting to 0.125% of the total melt mass of the alloy). This is consistent with the experiments reported by JUNG et al [15]. After that, before pouring into stainless steel metal mould, the melt is allowed to soak for about 15 min to entirely feel the effects of grain modifier and refiner. During the experiments, depending on the melt quantity and amount of superheat, a 40–50 °C drop in temperature is normally noticed while transferring the molten alloy from electric resistance furnace to the metal mould. This ascertains the necessity of holding such an elevated temperature in the heating furnace.

2.3 Slurry production and temperature measurements

For each experiment, about 1.5 kg of molten alloy is taken from the furnace and then transferred into a tundish. The molten alloy temperature in the tundish is frequently monitored by means of K-type mineral insulated (MI) twisted-pair thermocouples from UK based TC Ltd.

Molten alloy at a temperature of 625 °C is slowly poured at 0.025 kg/s flow rate into the metal mould via three different stainless steel oblique plates (of lengths 200, 250 and 300 mm) kept at 60° plate inclination with three different water flow rates of 2.5, 7.5 and 10 L/min (involving plate cooling rates corresponding to 1000, 2000 and 2500 W/(m²·K)) underneath it. The temperature of semisolid slurry collected at the plate exit is also noted on a regular basis.

2.4 Semisolid billet casting and induction reheating

The billets of length 250 mm and diameter 60 mm are cast by quenching semisolid slurry in the stated metal mould. For relative comparison of microstructures, some of the semisolid cast billets are also reheated up to 580 °C (i.e., slightly above solidus temperature) in an induction furnace. This induction reheating involves isothermal holding of semisolid-cast billets at a temperature slightly above the solidus temperature of the metal alloy.

2.5 Specimen preparation

Small sections are sliced from the cast/reheated billets to form 15 mm thick disks. For metallographic analysis, all the sliced samples are polished by emery papers of different grades, subsequently followed by SiC powder polishing together with diamond paste polishing. Each of the polished specimens obtained by the already described procedure are etched using Keller's reagent (1 mL HF, 1.5 mL HCl, 2.5 mL HNO₃ and 100 mL H₂O) at the ambient temperature.

2.6 Microstructure morphology and characterization

Optical microscopy and image analysis software are used to enumerate and measure the heterogeneity in microstructural morphology. The micrograph images of samples are then snapped at the centre, middle and edge for characterization with image analysis using Leitz optical microscope for quantitative and metallographic analysis. Sigma Scan Pro image (version 4.0) analysis software is deployed for quantitative metallographic analysis such as for determining the area and perimeter of primary α -phase particles. The microstructural characterizations of the snapped images are done based on the under-mentioned parameters:

1) Fraction of primary α -phase (%): It is determined in accordance with the area ratio of primary α -phase and eutectic Si phase.

2) Grain size: It is estimated by the intercept method.

3) Shape factor: It is a measure of globularity of the primary α -phase. It is evaluated by the formula $S=4\pi A/P^2$, where A and P are area and perimeter of the primary α -phase, respectively. For an ideal circle, the value is 1,

and for a dendrite, the formula yields a value tending to be zero. For a rosette structure, depending on the amount and degree of irregularity, it yields a value between 0 and 1.

4) Particle density: Otherwise termed as grain density, it is the number of primary α -phase globules per unit area; with the increase of this number, the amount and degree of dendrite multiplication or breakdown are superior.

3 Results and discussion

Thorough experiments are performed to investigate the influences of plate length and plate cooling rate on solidification and microstructure of both semisolid-cast and heat-treated billets. Initially, molten A356 aluminum alloy at 625 °C is poured at 0.025 kg/s flow rate on an oblique plate of length 250 mm, inclination 60° with 7.5 L/min water flow rate below it.

3.1 Effect of plate length

To investigate the influence of plate length on solidification and microstructure, controlled experiments are performed under the stated experimental conditions at three different plate lengths (200, 250 and 300 mm). Since longer plate length involves more residence time (or solidification time) of the melt flowing down on the oblique plate, the slurry temperature at plate exit decreases with plate length. Eventually, it results in higher solid fraction with longer plate length. Table 2 gives average temperature and solid fraction data of A356 semisolid slurry collected at the plate exit and obtained from the experiments conducted at three different plate lengths.

Table 2 Effect of plate length on temperature and solid fraction data of A356 semisolid slurry collected at plate exit

Plate length/ mm	$t_{\text{exit}}/^\circ\text{C}$	Solid fraction from Scheil equation/%
200	610	18
250	607	24
300	603	30

3.1.1 Microstructure morphology of semisolid-cast billets

Accordingly, three different semisolid cast-billets are produced at the stated plate lengths. The representative samples are prepared to snap micrograph images at the centre, middle and edge using Leitz optical microscope for quantitative and metallographic analysis.

Figure 1 highlights and compares the representative microstructures of the semisolid-cast billets produced at three different plate lengths. It may be observed that the primary α -phase particles are normally smaller for longer plate length. This may be due to the fact that the

semisolid slurry collected at plate exit and entering the metal mould contains more fractions of primary α -phase particles for longer plate length. More residence time (or solidification time) causes initiation of more nucleation sites (on the plate wall) for grain growth, dendrite fragmentation, breakage along with its transport. Ultimately, it results in more fractions of primary α -phase particles at plate exit. There are growth, spheroidization and microstructure refinement in the metal mould as well. Figure 1 also illustrates the radial variations in microstructure of the stated semisolid-cast billets from globular at centre to dendritic at edge through rosette-like at middle. It can be owing to non-uniform cooling, i.e., faster cooling at the wall of metal mould and slower cooling at the centre.

This demonstrates that the evolution of microstructure certainly depends on plate length. The results from the measurement of the grain size of α -phase particles, shape factors, eutectic fractions and the grain or particle densities along the radial direction of the billets are summarized in Fig. 2.

3.1.2 Microstructure characterization of semisolid-cast billets

Figure 2 highlights the microstructural characteristics observed or measured along with their variations. It depicts that for longer plate length, the average grain size of α -particle is smaller, whereas, shape factor, fraction of primary α -phase and grain density are larger. More residence time (or solidification time) on the plate wall causes more dendritic fragmentation and breakage along with its transport, resulting in the evolution of relatively fine microstructure. Figure 2 also illustrates the non-uniformity of the microstructural characteristics in the radial direction. It shows decrease in grain size, shape factor, fraction of primary α -phase and increase in grain density in radially outward direction (from centre to edge of the stated semisolid cast billets).

For the oblique plate semisolid-cast billet with 200 mm plate length, the average grain size decreases from 77 μm at the centre to 36 μm at the edge through 71 μm at the middle (Fig. 2(a)). Correspondingly, the shape factor decreases from 0.66 at the centre to 0.26 at the edge through 0.62 at middle (Fig. 2(b)), and the primary α -phase fraction decreases from 0.68 at the centre to 0.50 at the edge through 0.64 at the middle (Fig. 2(c)). The grain or particle density increases from 191 mm^{-2} at the centre to 380 mm^{-2} at edge through 203 mm^{-2} at the middle (Fig. 2(d)). Likewise, for the billets cast with other plate lengths (250 mm and 300 mm), the variations of average grain size, shape factor, primary α -phase fraction, and grain density follow a similar trend as shown in Fig. 2.

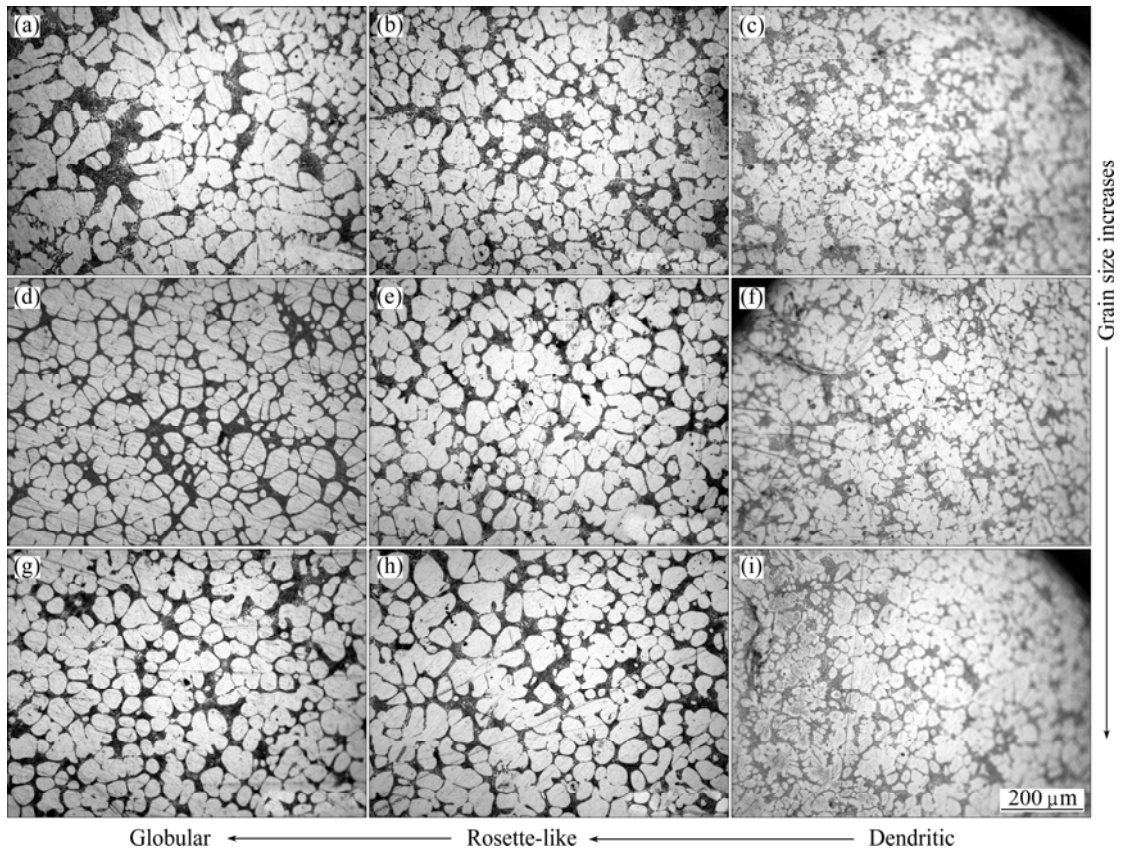


Fig. 1 Micrographs of semisolid-cast billets produced at different plate lengths: (a) 200 mm, centre; (b) 200 mm, middle; (c) 200 mm, edge; (d) 250 mm, centre; (e) 250 mm, middle; (f) 250 mm, edge; (g) 300 mm, centre; (h) 300 mm, middle; (i) 300 mm, edge

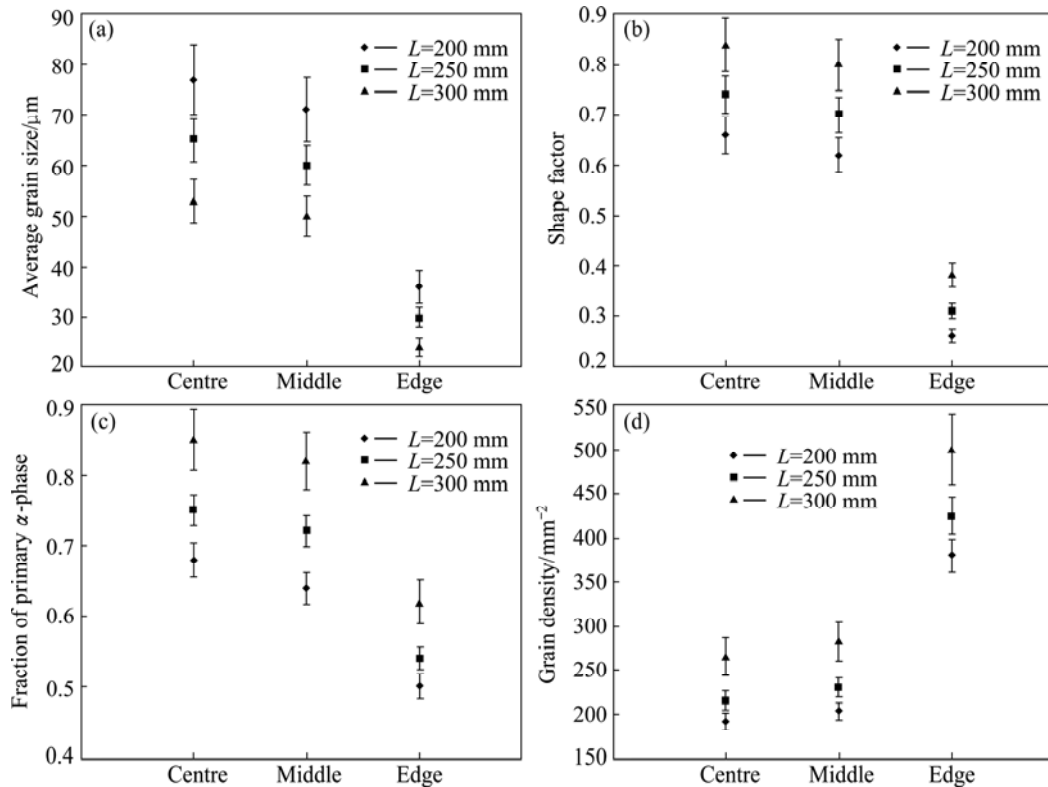


Fig. 2 Microstructure characterization of semisolid-cast billets produced at different plate lengths: (a) Grain size vs location; (b) Shape factor vs location; (c) Primary α -phase fraction vs location; (d) Grain density vs location

This demonstrates that the plate length definitely influences the final microstructure of the semisolid-cast billets which, in turn, affects average grain size, shape factor, fraction of α -phase, and particle or grain density.

3.1.3 Microstructure morphology of heat-treated billets

To improve the surface quality, the stated semisolid-cast billets are reheated up to slightly above solidus temperature (580 °C) by induction heating. The representative samples are prepared from the heat-treated billets to snap micrograph images at the centre, middle and edge using Leitz optical microscope for quantitative and metallographic analysis.

Figure 3 shows the representative microstructures of the heat-treated billets produced. Here, nearly uniform and globular microstructure is observed from centre to edge of each heated-treated billet. It may be due to the temperature uniformity from the centre to edge of the billets because of isothermal holding in the induction furnace for about 10 min. However, the primary α -phase particles are observed to be still finer for longer plate length.

This demonstrates that the microstructure morphology certainly gets improved because of induction heating. The results from the measurement of

the grain size of α -phase particles, shape factors, primary α -phase fractions and the grain or particle densities along the radial direction of the heat billets are summarized in Fig. 4.

3.1.4 Microstructure characterization of heat-treated billets

Figure 4 compares the results obtained from the measurements of grain sizes, shape factors, eutectic fractions and grain densities from the samples of the said semisolid-cast and heat-treated billets. The average grain size, shape factor, fraction of primary α -phase and grain density are found to be nearly uniform from centre to edge of each heat-treated billet. However, the trends of variations in average grain size, shape factor, fraction of primary α -phase and grain density with plate length are the same for both the said billets. Also, it may be observed that the average grain size, shape factor and fraction of primary α -phase increase with induction reheating, whereas, grain density decreases. It may be due to the fact that the particle coalescence occurs during isothermal holding causing amalgamation of small particles into larger ones. The particle coalescence also leads to liquid entrapment in primary α -phase which is also observed in some cases.

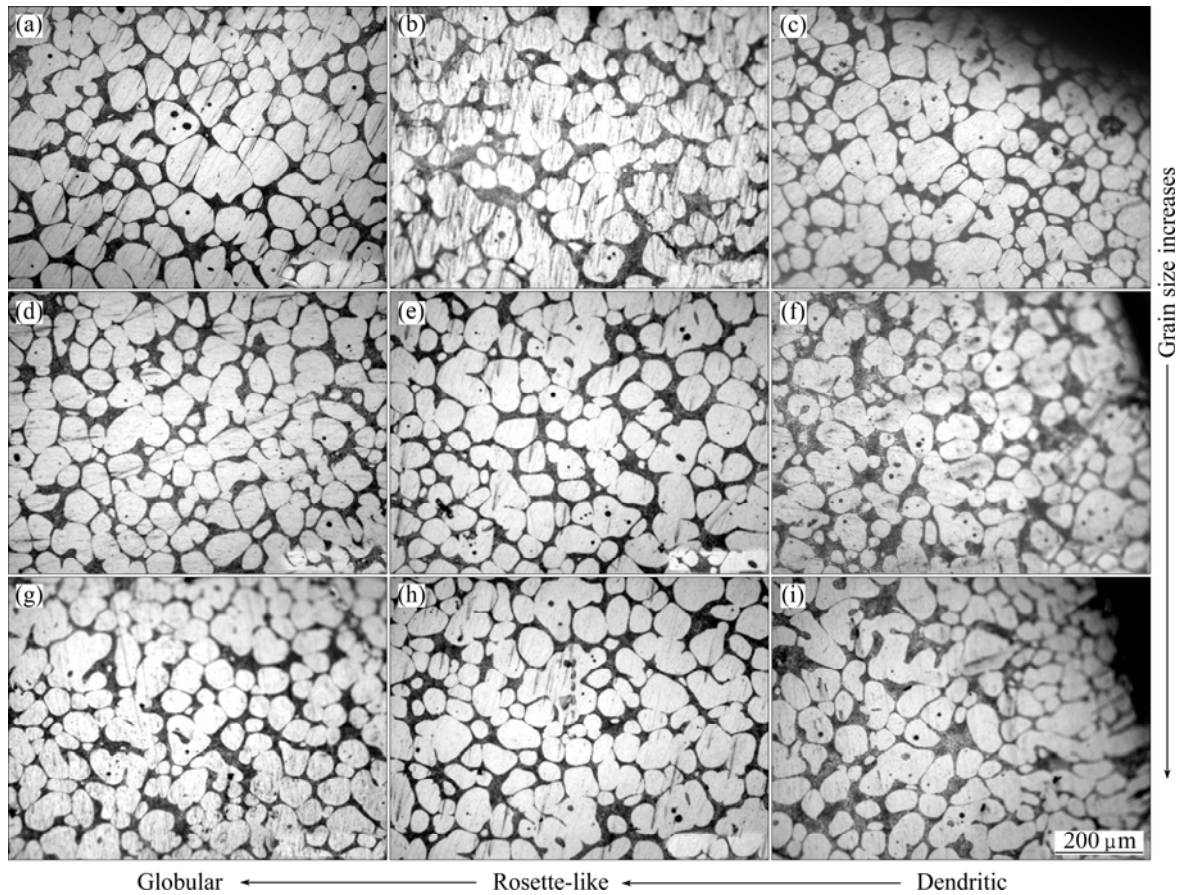


Fig. 3 Micrographs of heat-treated billets produced at different plate lengths after isothermal holding: (a) 200 mm, centre; (b) 200 mm, middle; (c) 200 mm, edge; (d) 250 mm, centre; (e) 250 mm, middle; (f) 250 mm, edge; (g) 300 mm, centre; (h) 300 mm, middle; (i) 300 mm, edge

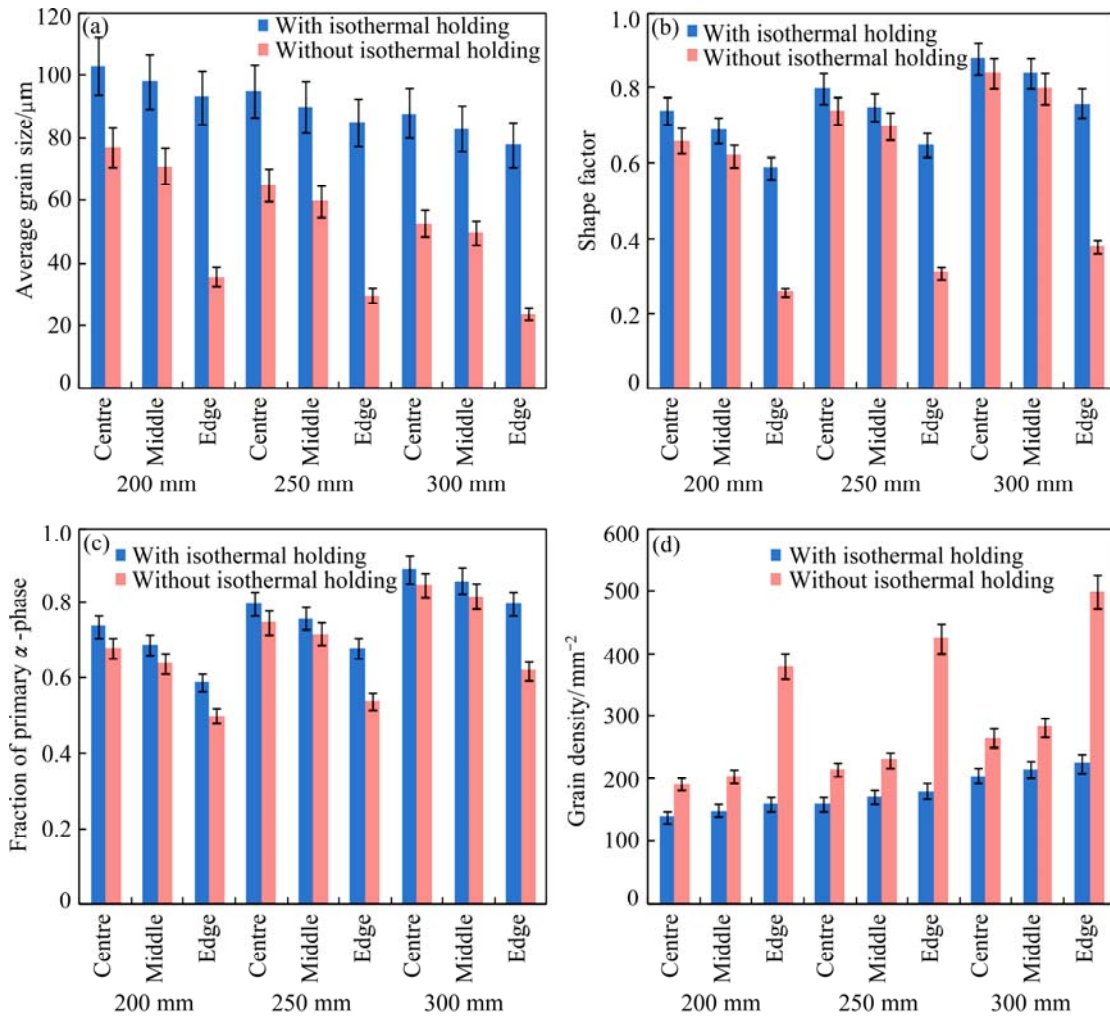


Fig. 4 Microstructure characterization of heat-treated billets produced at different plate lengths before and after isothermal holding: (a) Grain size vs location; (b) Shape factor vs location; (c) Primary α -phase fraction vs location; (d) Grain density vs location

Due to isothermal holding of the semisolid-cast billet produced at 200 mm plate length, the average grain size increases from 77 μm to 103 μm at the centre, and 36 μm to 93 μm at the edge through 71 μm to 98 μm at the middle (Fig. 4(a)). Correspondingly, the shape factor increases from 0.66 to 0.74 at the centre, and 0.26 to 0.59 at the edge through 0.62 to 0.69 at the middle (Fig. 4(b)). The primary α -phase fraction increases from 0.68 to 0.74 at the centre, and 0.50 to 0.59 at the edge through 0.64 to 0.69 at the middle (Fig. 4(c)). Also, the grain or particle density decreases from 191 to 140 mm^{-2} at the centre, and 380 to 160 mm^{-2} at edge through 203 to 150 mm^{-2} at the middle (Fig. 4(d)). Likewise, as shown in Fig. 4, the variations of average grain size, shape factor, primary α -phase fraction, and grain density follow a similar trend for the billets cast with other plate lengths (250 mm and 300 mm).

This clearly demonstrates that the heat treatment of semisolid-cast billets involving isothermal holding (slightly above the solidus temperature of A356 alloy)

certainly affects the final microstructure of the billets, which, in turn, influences the average grain size, shape factor, fraction of α -phase, and particle or grain density.

3.2 Effect of plate cooling rate

With the stated experimental conditions, in order to investigate the influence of plate cooling rate on solidification and microstructure, controlled experiments are conducted at plate cooling rates corresponding to three different heat transfer coefficients (1000, 2000, 2500 $\text{W}/(\text{m}^2\cdot\text{K})$). Since higher plate cooling rate involves higher solidification rate/extent or amount of solidification of the melt flowing down on the oblique plate, the slurry temperature at plate exit decreases with plate cooling rate increasing. Eventually, it results in higher solid fraction at higher plate cooling rate. Table 3 gives average temperature and solid fraction data of A356 semisolid slurry collected at the plate exit and obtained from the experiments conducted at three different heat transfer coefficients.

Table 3 Temperature and solid fraction data of A356 semisolid slurry collected at plate exit at different plate cooling rates

Heat transfer coefficient/ ($\text{W}\cdot\text{m}^{-2}\cdot\text{K}^{-1}$)	$t_{\text{exit}}/^\circ\text{C}$	Solid fraction from Scheil equation/%
1000	614	10
2000	607	24
2500	603	30

3.2.1 Microstructure morphology of semisolid-cast billets

Accordingly, three different semisolid-cast billets are produced at the stated plate cooling rates. The representative samples are prepared to snap micrograph images at the centre, middle and edge using Leitz optical microscope for quantitative and metallographic analysis.

Figure 5 highlights and compares the representative microstructures of the semisolid-cast billets produced at three different plate cooling rates. It may be observed that the primary α -phase particles are normally smaller for higher plate cooling rate. This may be due to the fact that the semisolid slurry collected at the plate exit and the entering of the metal mould contains higher fractions of primary α -phase particles for higher plate cooling rate. Higher solidification rate (extent or amount of

solidification) causes initiation of more nucleation sites (on the plate wall) for grain growth, dendrite fragmentation, breakage along with its transport. Ultimately, it results in more fractions of primary α -phase particles at plate exit. There are growth, spheroidization and microstructure refinement in the metal mould as well. Figure 5 also illustrates the radial variations in microstructure of the stated semisolid cast billets from globular at centre to dendritic at edge through rosette-like at middle. It can be owing to non-uniform cooling, i.e., faster cooling at the wall of metal mould and slower cooling at the centre.

This demonstrates that the evolution of microstructure certainly depends on plate cooling rate, apart from the plate length. The results from the measurement of the grain size of α -phase particles, shape factors, eutectic fractions and the grain or particle densities along the radial direction of the billets are summarized in Fig. 6.

3.2.2 Microstructure characterization of semisolid cast billets

Figure 6 shows the microstructural characteristics observed or measured along with its variations. It depicts that for higher plate cooling rate, the average grain size

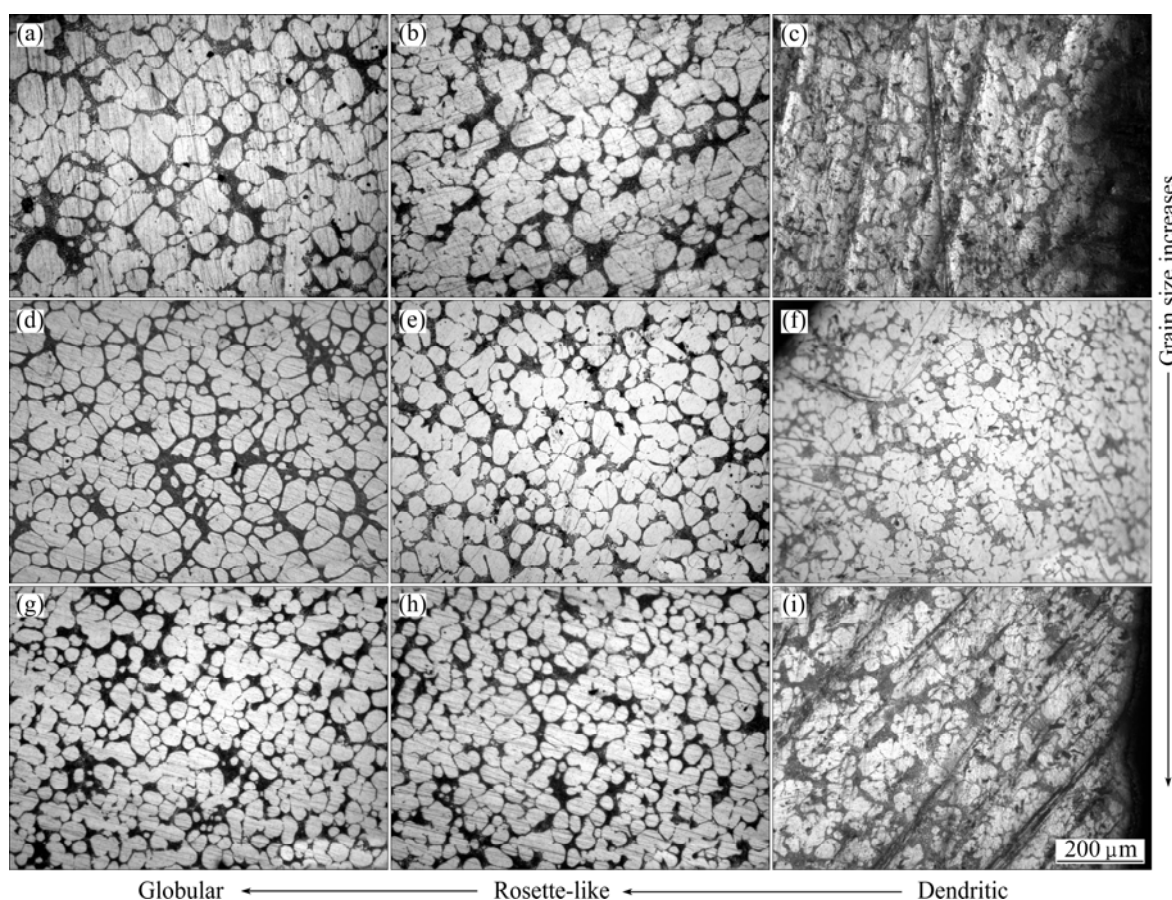


Fig. 5 Micrographs of semisolid-cast billets produced at different heat transfer coefficients: (a) $h=1000 \text{ W}/(\text{m}^2\cdot\text{K})$, centre; (b) $h=1000 \text{ W}/(\text{m}^2\cdot\text{K})$, middle; (c) $h=1000 \text{ W}/(\text{m}^2\cdot\text{K})$, edge; (d) $h=2000 \text{ W}/(\text{m}^2\cdot\text{K})$, centre; (e) $h=2000 \text{ W}/(\text{m}^2\cdot\text{K})$, middle; (f) $h=2000 \text{ W}/(\text{m}^2\cdot\text{K})$, edge; (g) $h=2500 \text{ W}/(\text{m}^2\cdot\text{K})$, centre; (h) $h=2500 \text{ W}/(\text{m}^2\cdot\text{K})$, middle; (i) $h=2500 \text{ W}/(\text{m}^2\cdot\text{K})$, edge

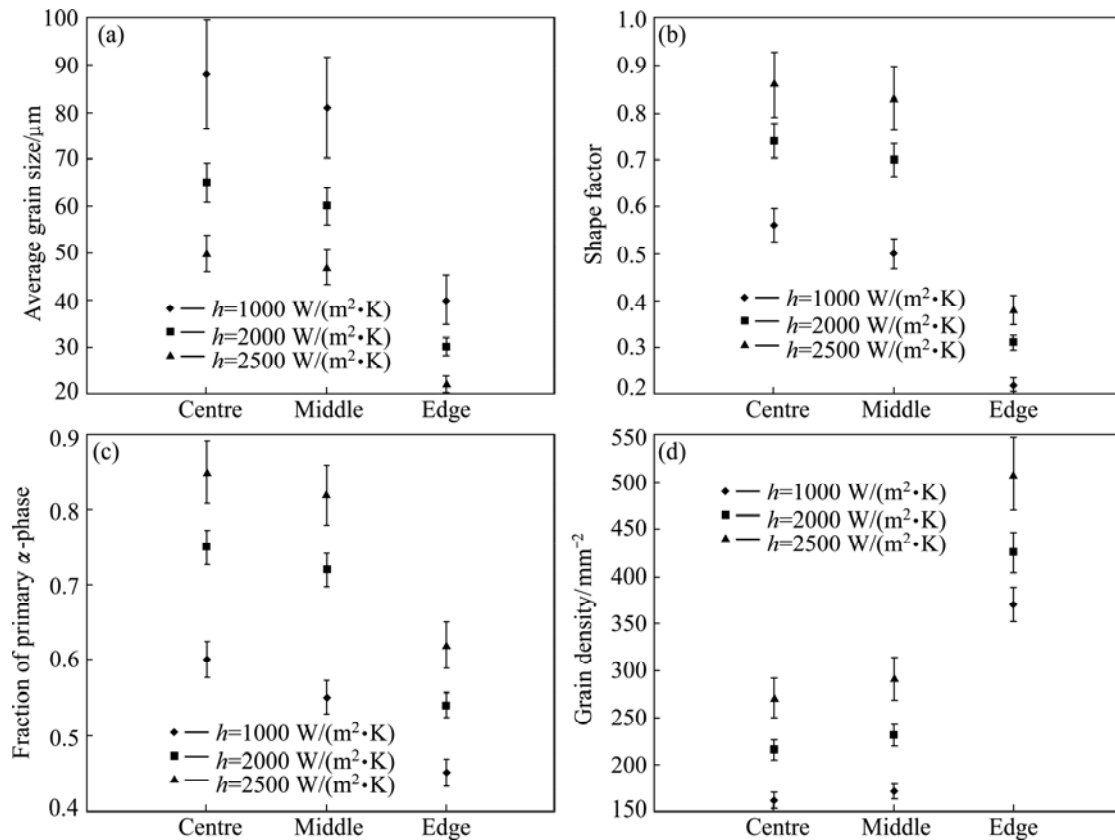


Fig. 6 Microstructure characterization of semisolid-cast billets produced at different heat transfer coefficients: (a) Grain size vs location; (b) Shape factor vs location; (c) Grain size vs location; (d) Shape factor vs location

of α -phase particle is less, whereas, shape factor, fraction of primary α -phase and grain density are more. Higher solidification rate (extent or amount of solidification) on the plate wall causes more dendritic fragmentation, breakage along with its transport, resulting in the evolution of relatively fine microstructure. Figure 6 also illustrates the non-uniformity of the microstructural characteristics in the radial direction. It shows decrease in grain size, shape factor, fraction of primary α -phase and increase in grain density in radially outward direction (from centre to edge of the stated semisolid cast billets).

For the oblique plate semisolid-cast billet with plate cooling rate corresponding to heat transfer coefficient of $1000 \text{ W}/(\text{m}^2\cdot\text{K})$, the average grain size decreases from $88 \mu\text{m}$ at the centre to $40 \mu\text{m}$ at the edge through $81 \mu\text{m}$ at the middle (Fig. 6(a)). Correspondingly, the shape factor decreases from 0.56 at the centre to 0.22 at the edge through 0.50 at middle (Fig. 6(b)), and the primary α -phase fraction decreases from 0.60 at the centre to 0.45 at the edge through 0.55 at the middle (Fig. 6(c)). The grain or particle density increases from 160 mm^{-2} at the centre to 370 mm^{-2} at edge through 170 mm^{-2} at the middle (Fig. 6(d)). Likewise, for the billets cast with other plate cooling rates (2000 and $2500 \text{ W}/(\text{m}^2\cdot\text{K})$), the variations of average grain size, shape factor, primary

α -phase fraction, and grain density follow a similar trend as shown in Fig. 6.

This demonstrates that the plate cooling rate definitely influences the final microstructure of the semisolid-cast billets which, in turn, affects average grain size, shape factor, fraction of α -phase, and particle or grain density.

3.2.3 Microstructure morphology of heat-treated billets

To improve the surface quality, the stated semisolid cast billets are reheated up to slightly above solidus temperature ($580 \text{ }^\circ\text{C}$) by induction heating. The representative samples are prepared from the heat-treated billets to snap micrograph images at the centre, middle and edge using Leitz optical microscope for quantitative and metallographic analysis.

Figure 7 demonstrates the representative microstructures of the heat-treated billets produced. Here, nearly uniform and globular microstructure is observed from centre to edge of each heated treated billet. It may be due to the temperature uniformity from the centre to edge of the billets because of isothermal holding in the induction furnace for about 10 min. However, the primary α -phase particles are observed to be still smaller for higher plate cooling rate.

This demonstrates that the microstructure morphology certainly gets improved because of the

induction heating. The results from the measurement of the grain size of α -phase particles, shape factors, primary α -phase fractions and the grain or particle densities along the radial direction of the heat-treated billets are summarized in Fig. 8.

3.2.4 Microstructure characterization of heat-treated billets

Figure 8 compares the results obtained from the measurements of grain size, shape factor, eutectic fraction and the grain density from the samples of the semisolid-cast and heat-treated billets. The average grain size, shape factor, fraction of primary α -phase and grain density are found to be nearly uniform from centre to edge of each heat-treated billet. However, the trends of variations in average grain size, shape factor, fraction of primary α -phase and grain density with plate cooling rate are the same for both the said billets. Also, it may be observed that the average grain size, shape factor and fraction of primary α -phase increase with induction reheating, whereas, grain density decreases with the same. It may be due to the fact that the particle coalescence occurs during isothermal holding, causing amalgamation of small particles into bigger ones. The particle coalescence also leads to liquid entrapment in primary α -phase which is also observed in some cases.

Due to isothermal holding of the semisolid cast billet produced at plate cooling rate corresponding to heat transfer coefficient of $2000 \text{ W}/(\text{m}^2\cdot\text{K})$, the average grain size increases from $88 \mu\text{m}$ to $109 \mu\text{m}$ at the centre, and $40 \mu\text{m}$ to $99 \mu\text{m}$ at the edge through $81 \mu\text{m}$ to $104 \mu\text{m}$ at the middle (Fig. 8(a)). Correspondingly, the shape factor increases from 0.56 to 0.64 at the centre, and 0.22 to 0.49 at the edge through 0.50 to 0.59 at the middle (Fig. 8(b)). The primary α -phase fraction increases from 0.60 to 0.66 at the centre, and 0.45 to 0.51 at the edge through 0.55 to 0.61 at the middle (Fig. 8(c)). Also, the grain or particle density decreases from 160 mm^{-2} at the centre, and 370 to 110 mm^{-2} at edge through 170 to 100 mm^{-2} at the middle (Fig. 8(d)). Likewise, as shown in Fig. 8, the variations of average grain size, shape factor, primary α -phase fraction, and grain density follow a similar trend for the billets cast with other plate cooling rates (corresponding to heat transfer coefficients of 2000 and $2500 \text{ W}/(\text{m}^2\cdot\text{K})$).

This clearly demonstrates that the heat treatment of semisolid-cast billets involving isothermal holding (slightly above solidus temperature of A356 alloy) certainly affects the final microstructure of the billets, which, in turn, influences average grain size, shape factor, fraction of α -phase, and particle or grain density.

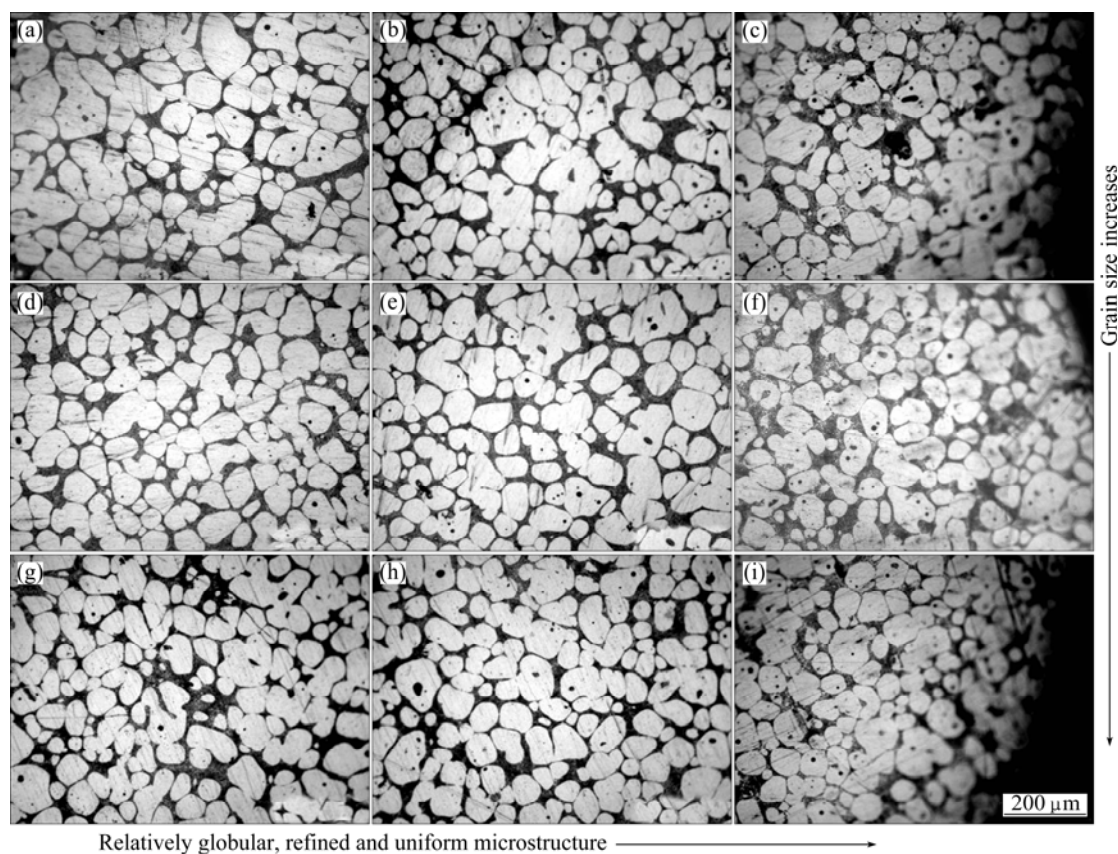


Fig. 7 Micrographs of heat-treated billets produced at different heat transfer coefficients after isothermal holding: (a) $h=1000 \text{ W}/(\text{m}^2\cdot\text{K})$, centre; (b) $h=1000 \text{ W}/(\text{m}^2\cdot\text{K})$, middle; (c) $h=1000 \text{ W}/(\text{m}^2\cdot\text{K})$, edge; (d) $h=2000 \text{ W}/(\text{m}^2\cdot\text{K})$, centre; (e) $h=2000 \text{ W}/(\text{m}^2\cdot\text{K})$, middle; (f) $h=2000 \text{ W}/(\text{m}^2\cdot\text{K})$, edge; (g) $h=2500 \text{ W}/(\text{m}^2\cdot\text{K})$, centre; (h) $h=2500 \text{ W}/(\text{m}^2\cdot\text{K})$, middle; (i) $h=2500 \text{ W}/(\text{m}^2\cdot\text{K})$, edge

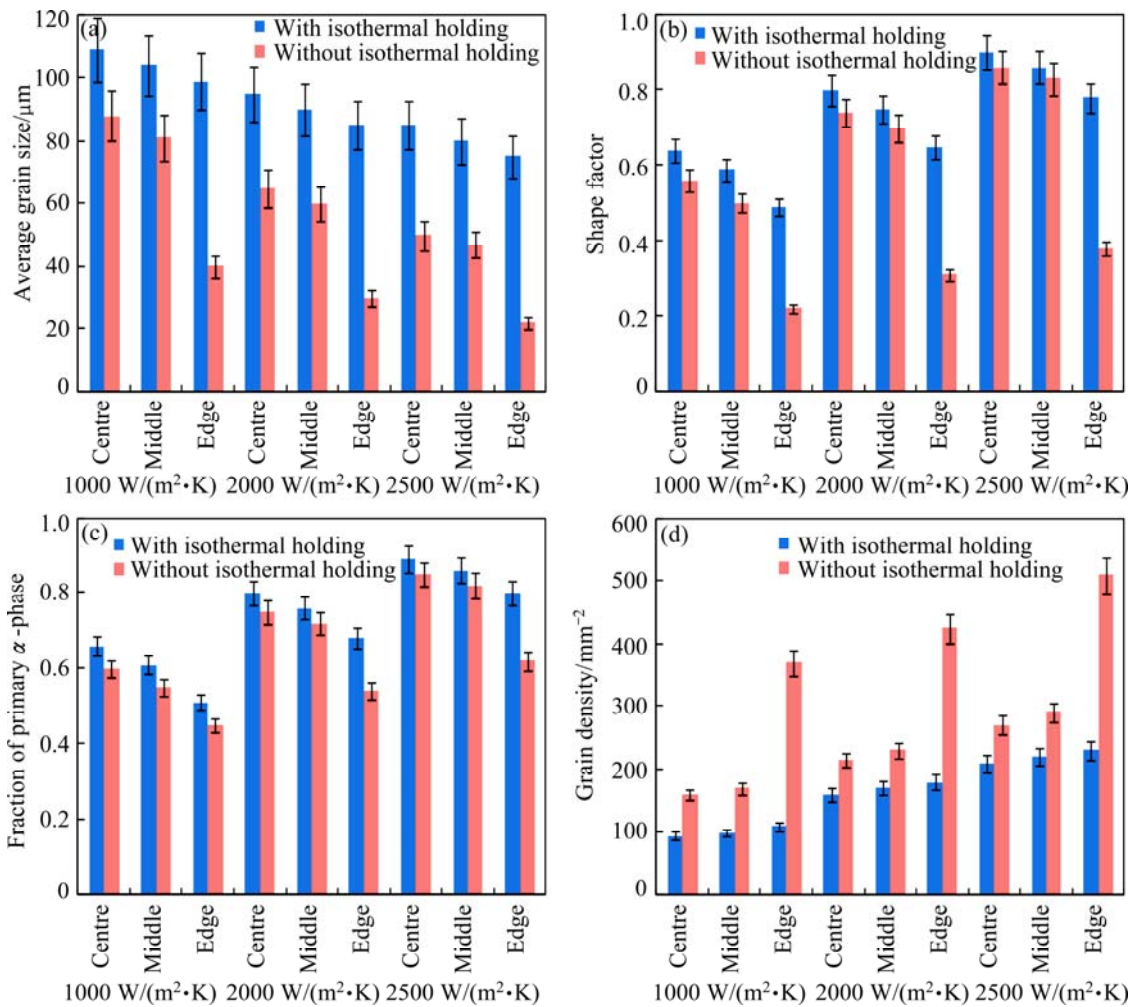


Fig. 8 Microstructure characterization of heat-treated billets produced at different heat transfer coefficients after isothermal holding: (a) Grain size vs location; (b) Shape factor vs location; (c) Primary α -phase fraction vs location; (d) Grain density vs location

4 Conclusions

1) Temperature of semisolid slurry at plate exit decreases with the increase in plate length/plate cooling rate. Solid fraction of slurry at plate exit increases with plate length/plate cooling rate. Grain size of primary α -phase particle decreases with the increase in plate length/plate cooling rate. Shape factor, fraction of primary α -phase and particle density increase with plate length/plate cooling rate increasing. These noticeable variations can be due to higher residence time (or solidification time) at higher plate length/plate cooling rate.

2) For the oblique plate semisolid-cast billet produced at 250 mm plate length and cooling rate corresponding to heat transfer coefficient of 2000 W/(m²·K), the average grain size decreases from 65 μm at the centre to 30 μm at the edge through 60 μm at the middle. Correspondingly, the shape factor decreases

from 0.74 at the centre to 0.31 at the edge through 0.7 at middle, and the primary α -phase fraction decreases from 0.75 at the centre to 0.54 at the edge through 0.72 at the middle. The grain density increases from 215 mm^{-2} at the centre to 425 mm^{-2} at edge through 230 mm^{-2} at the middle. Likewise, a similar trend follows for the billets cast with other plate lengths/plate cooling rates. This microstructural inhomogeneity can be due to non-uniform cooling from centre to edge of the billets.

3) Due to isothermal holding of the semisolid cast billet produced at 250 mm plate length and cooling rate corresponding to heat transfer coefficient of 2000 W/(m²·K), the average grain size increases from 65 μm to 95 μm at the centre, and 30 μm to 85 μm at the edge through 60 μm to 90 μm at the middle. Likewise, the shape factor increases from 0.74 to 0.8 at the centre, and 0.31 to 0.65 at the edge through 0.7 to 0.75 at the middle. The primary α -phase fraction increases from 0.75 to 0.80 at the centre, and 0.54 to 0.68 at the edge through 0.72 to 0.76 at the middle. Also, the grain density decreases from

215 to 160 mm⁻² at the centre, and 425 to 180 mm⁻² at edge through 230 to 170 mm⁻² at the middle. The trend is similar for the billets cast with other plate lengths/plate cooling rates. This can be a result of temperature uniformity across the entire domain of the billets during induction reheating.

4) With the stated experimental conditions, it is observed that the plate length of 250 mm associated with plate cooling rate corresponding to heat transfer coefficient of 2000 W/(m²·K) gives fine and globular microstructures and is the optimum one as there is absolutely no possibility of sticking of slurry to the plate wall. Because, longer plate length/higher plate cooling rate will prolong residence time or solidification time, resulting in higher solid fraction of slurry, causing slurry to become more viscous. Whereas, shorter plate length/lower plate cooling rate results in coarser microstructure on account of inadequate shearing.

Acknowledgments

The financial support received from Ministry of Mines, TIFAC, and Department of Science and Technology is gratefully acknowledged.

References

- [1] SPENCER D B, MEHRABIAN R, FLEMINGS M C. Rheological behavior of Sn–15%Pb in the crystallization range [J]. Metallurgical Transactions, 1972, 3: 1925–1932.
- [2] LAXMANAN V, FLEMINGS M C. Deformation of semisolid Sn–15%Pb alloy [J]. Metallurgical Transactions A, 1980, 11: 1927–1937.
- [3] CAMPBELL J. Effects of vibration during solidification [J]. International Materials Review, 1981, 2: 71–106.
- [4] FLEMINGS M C. Behavior of metal alloys in the semisolid state [J]. Metallurgical Transactions A, 1991, 22: 957–981.
- [5] KIRKWOOD D H. Semisolid metal processing [J]. International Materials Review, 1994, 39(5): 173–189.
- [6] FAN Z. Semisolid metal processing [J]. International Materials Review, 2002, 47(2): 49–85.
- [7] SUKUMARAN K, PAI B C, CHAKRABORTY M. The effect of isothermal mechanical stirring on an Al–Si alloy in the semisolid condition [J]. Materials Science and Engineering A, 2004, 369: 275–283.
- [8] NAFISI S, GHOMASHCHI R. Effect of string on solidification pattern and alloy distribution during semi-solid metal casting [J]. Materials Science and Engineering A, 2006, 437: 388–395.
- [9] LASHKARI O, GHOMASHCHI R. The implication of rheology in semi-solid metal process: An overview [J]. Journal of Material Processing Technology, 2007, 182(1–3): 229–240.
- [10] KUMAR P. Experimental investigation of rheocasting using linear electromagnetic stirring [D]. Bangalore: Indian Institute of Science, 2008.
- [11] BARMAN N. Studies on transport phenomena during solidification in presence of electromagnetic stirring [D]. Bangalore: Indian Institute of Science, 2008.
- [12] TAGHAVI F, SAGHAFIAN H, KHARRAZI Y H K. Study on the ability of mechanical vibration for the production of thixotropic microstructure in A356 aluminum alloy [J]. Materials and Design, 2009, 30(1): 115–121.
- [13] KUND N K, DUTTA P. Numerical simulation of solidification of liquid aluminum alloy flowing on cooling slope [J]. Transactions of Nonferrous Metal Society of China, 2010, 20(s3): s898–s905.
- [14] KUND N K, DUTTA P. Scaling analysis of solidification of liquid aluminum alloy flowing on cooling slope [J]. Transactions of Indian Institute of Metals, 2012, 65(6): 587–594.
- [15] JUNG B I, JUNG C H, HAN T K, KIM Y H. Electromagnetic stirring and Sr modification in A356 alloy [J]. Journal of Material Processing Technology, 2001, 111(1–3): 69–73.

板面长度和冷却速度对 A356 合金 斜板凝固过程与显微组织的影响

N. K. KUND

Department of Mechanical Engineering, Indian Institute of Science, Bangalore 560012, India

摘要: 当 A356 合金流经由底部反向水流冷却的斜板时将发生部分凝固。在板面上将连续形成柱状枝晶。由于强制对流作用, 这些枝晶将被剪切成等轴晶并被出口的半固态浆体冲刷。板面冷却速度可为高质量半固态浆体提供需要的凝固过程, 而板面长度可提供必需的剪切过程。将半固态浆体在金属模具中冷却以制备具有理想微观组织的半固态锭坯。此外, 对半固态铸造锭坯进行热处理以提高表面质量, 并对半固态铸造和热处理后锭坯的微观组织进行对比。研究板面长度和板面冷却速度对斜板冷却锭坯凝固过程和显微组织的影响。三种板面长度(200, 250, 300 mm)分别对应不同传热系数(1000, 2000 和 2500 W/(m²·K))。最佳板面长度和相应的传热系数分别为 250 mm 和 2000 W/(m²·K), 在此条件下, 由于没有浆体附着在板面上, 锭坯具有细小的球状组织。

关键词: 铝合金; 斜板; 浆体; 显微组织; 板面长度; 板面冷却速度

(Edited by Yun-bin HE)